Chemical Fingerprint Assessment of Surface Resistance in Silicone Rubber Insulators Using Coal Fly Ash as Filler

Harjib Haridh
Master Program in Electrical Engineering, Faculty of Electricity and Renewable Energy, PLN Institute of Technology, Jakarta, Indonesia

Syamsir Abduh
Department of Electrical Engineering, Faculty of Electricity and Renewable Energy, PLN Institute of Technology, Jakarta, Indonesia

Christiono
Department of Electrical Engineering, Faculty of Electricity and Renewable Energy, PLN Institute of Technology, Jakarta, Indonesia

Abstract: To support the infrastructure targets of Indonesia's PLN Electricity Supply Business Plan (RUPTL) 2025–2034 while managing abundant coal fly ash waste, this study investigates CFA valorization as a functional filler in silicone rubber insulators. Addressing the need for sustainable grid expansion, the research primarily focuses on the relationship between FTIR-derived chemical descriptors, CFA composition, and composite surface resistance. Chemical fingerprinting analysis demonstrates that CFA with high SiO_2 content (42.0%) better supports the composite's siloxane networks compared to iron-rich variants. Statistical modeling (adjusted $R^2 > 0.92$) confirms filler concentration as the primary predictor of resistance ($p < 0.001$). Optimal structural stability was associated with a 2:1 stoichiometric ratio of dimethyl groups—directly attached to the central silicon atoms ($Si(CH_3)_2$)—relative to the Si-O-Si backbone. Furthermore, a critical percolation threshold was identified at 70% filler concentration, beyond this loading level the integrity of the fundamental PDMS polymer structure is compromised, resulting in deteriorated insulator performance. These findings suggest that FTIR-based chemical fingerprinting has the potential to serve as an effective quality control framework, offering a scientifically grounded, sustainable material alternative in direct alignment with RUPTL strategic objectives.

Keywords: Silicone Rubber Composite, Coal Fly Ash Filler, Surface Resistance, Multiple Linear Regression.

Correspondents Author:
Christiono, Department of Electrical Engineering, Institut Teknologi Perusahaan Listrik Negara, Jakarta, Indonesia
Email: christiono@itpln.ac.id

Received June 1 2026; Revised July 12, 2026; Accepted July 12 2026; Published July 13, 2026.

Introduction

The escalating generation of coal fly ash (CFA) in Indonesia reaching approximately 9.8 million tons in 2019 alone presents severe ecological and public health challenges due to its hazardous heavy metal constituents, including lead (Pb), cadmium (Cd), arsenic (As), and mercury (Hg) (Chinara Abinawa & Alieftiyani Paramita Gobel, 2024; DJMB, 2021, Asof et al., 2022; Tambunan, 2022). Traditional, unsustainable management methods like open dumping aggravate these environmental risks (Ferdyanto & Afriandini, 2023). However, because CFA is characterized by a high presence of metal oxides, notably silica (SiO_2), alumina (Al_2O_3), iron oxide (Fe_2O_3), and calcium oxide (CaO), this rich silica content turns an environmental liability into a valuable asset for industrial utilization (Nurfitria & Febriyantiningrum, 2023). While CFA serves as a critical functional filler to partially substitute cement in concrete, geopolymers, and paving blocks within civil engineering (Apriyanti et al., 2024; Purnamasari et al., 2025; Rafrita et al., 2023; Syahputra et al., 2023), its application in high-voltage electrical insulation materials represents a more specialized and less explored domain.

In electrical engineering, insulation systems represent the backbone of power grid infrastructure, where high-voltage insulators must withstand intense electrical stress, environmental pollution, and mechanical loads to prevent flashovers (Syamsir Abduh., 2003). Polymer insulators based on room-temperature vulcanized (RTV) silicone rubber (SiR) are increasingly preferred over conventional porcelain and glass due to their hydrophobic properties, lightweight nature, and environmental resistance (C. Christiono, 2017; K.Kar., 2022). The incorporation of mineral fillers like aluminium trihydrate (ATH) and, more recently, CFA, modifies the electrical, mechanical, and chemical properties of the composite. Foundational and subsequent research has established that the dielectric and surface resistance properties of CFA-filled SiR composites depend critically on the filler's loading level (0–80 wt%) and source-specific chemical composition (C. Christiono, 2017; R. Christiono et al., 2023; Ikhlas Kitta et al., 2016; Kitta et al., 2016a; Kitta et al., 2016b; Roesdiono et al., 2025)

Optimization of these macro-properties has been attempted using response surface methodology (Thahara et al., 2023) and mechanical characterization (Fikri et al., 2024). Furthermore, although Fourier-transform infrared (FTIR) spectroscopy has been utilized to identify spectral shifts in Si-O-Si and $Si(CH_3)_2$ bands as qualitative aging markers in silicone rubber (Fan et al., 2018; Yang et al., 2021; Zhang et al., 2012), a systematic quantitative framework linking molecular-level chemical structure to macroscopic electrical performance has not been fully established. Crucially, none of these prior studies applied regression-based predictive modelling using FTIR spectral features as independent variables to predict surface

resistance directly. Prior material evaluations have relied on destructive electrical testing, which treats the internal interactions between the filler and the polymer matrix as a black box and fails to capture how variations in filler sources such as high SiO_2 ash from power plants versus high Fe_2O_3 ash from cement factories alter the fundamental polymer network.

To move beyond descriptive, post-fabrication destructive testing, a non-destructive, molecular-level quality control instrument is required to accurately identify chemical markers, such as the degradation of the polydimethylsiloxane (PDMS) structural matrix or critical percolation thresholds, before full-scale deployment in the power grid. This study introduces a predictive chemical fingerprinting approach that mathematically binds microscopic chemical descriptors directly to macroscopic electrical performance.

This study addresses this gap by: (i) characterizing two industrially relevant fly ash sources (CFAS-A from a large Coal-Fired Power Plant and CFAS-B from a cement factory) using X-ray Fluorescence (XRF) and FTIR spectroscopy; (ii) developing Multiple Linear Regression (MLR) models to predict surface resistance directly from FTIR-derived molecular descriptors; and (iii) introducing stoichiometric ratio analysis of the dimethyl silyl group $Si(CH_3)_2$ to the siloxane bridge Si-O-Si (ideally 2:1 in intact PDMS) as a novel quality control indicator for composite insulator manufacturing.

Research Method

This study investigates the effect of fly ash fillers on the electrical and chemical properties of silicone rubber (SiR) insulators through a structured experimental and statistical workflow. The methodology comprises four sequential phases: raw material characterization, sample preparation, experimental testing, and statistical modelling. First, two distinct coal fly ash sources—derived from a coal-fired power plant (CFPP) and a cement factory were characterized using X-ray Fluorescence (XRF) spectrometry. Next, these fillers were incorporated into an RTV-683 silicone rubber matrix at various weight fractions to fabricate composite insulator specimens. Electrical and chemical performance data were then collected via Surface Resistance testing (ASTM D257) and Fourier-Transform Infrared (FTIR) spectroscopy, respectively. Finally, a robust statistical framework was implemented, utilizing multiple linear regression (MLR), backward elimination, and interaction analysis to model the correlation between FTIR chemical features and surface resistance, followed by residual diagnostics and comparative validation. The overall workflow of this methodology, spanning from initial raw material characterization to final model validation, is systematically illustrated in the flowchart in Figure 1.

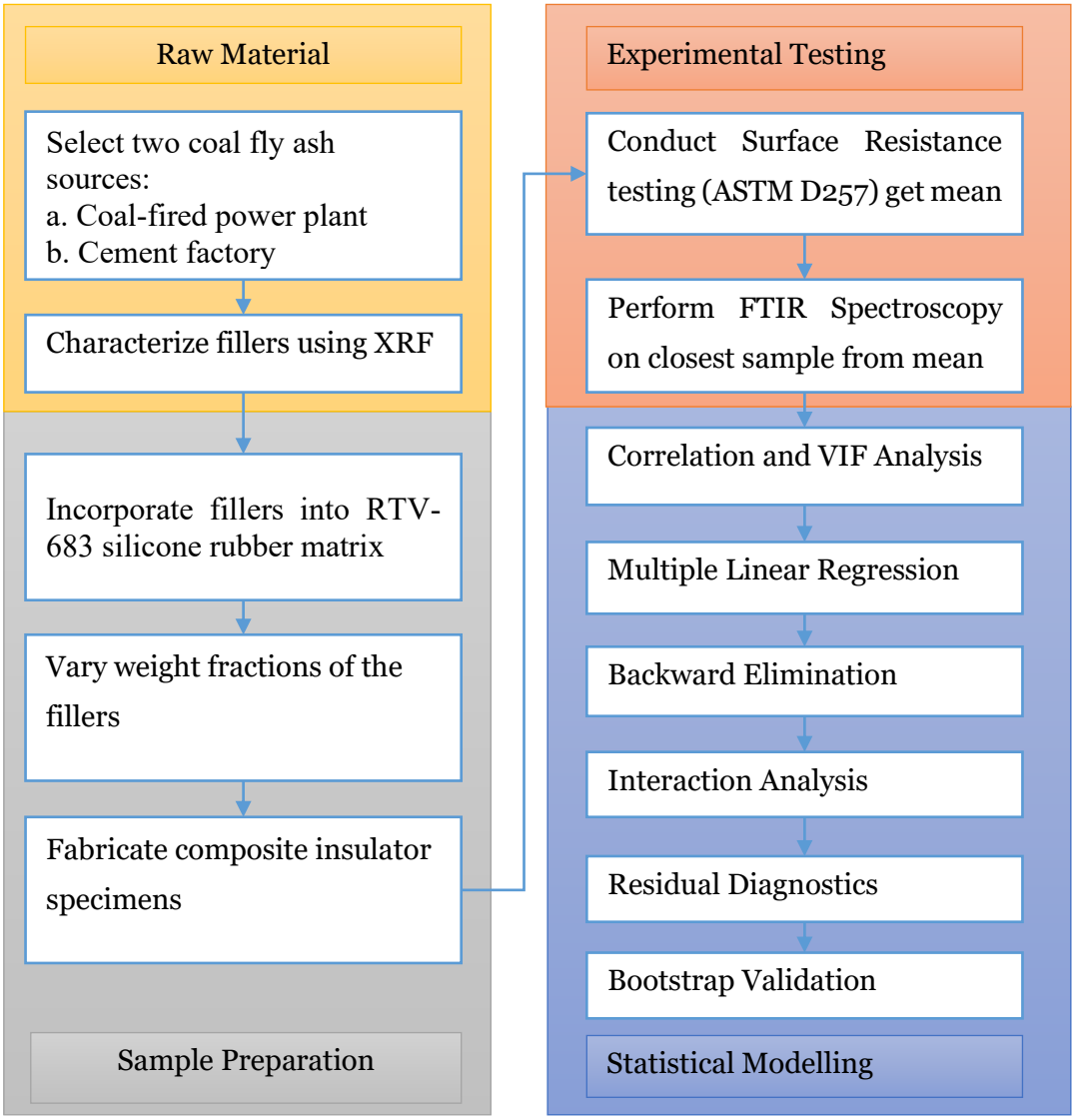

Figure 1 Research Framework: From Raw Material Characterization to Statistical Modelling

Fly Ash Characterization

Two coal fly ash sources were used as fillers: CFAS-A, obtained from a large coal-fired power plant in the Suralaya region, and CFAS-B, obtained from a cement manufacturing facility in Bekasi. Chemical compositions were determined using X-ray Fluorescence (XRF) spectrometry (Bruker S1 Titan). The composite samples were designated SRF-A (SiR + CFAS-A) and SRF-B (SiR + CFAS-B).

Sample Preparation

Silicone rubber composite specimens were prepared by incorporating fly ash fillers at nine loading concentrations: 0%, 10%, 20%, 30%, 40%, 50%, 60%, 70%, and 80% by weight. The base matrix was RTV-683 silicone rubber. The filler was mixed into the base matrix via mechanical stirring and then uniformly degassed using a vacuum chamber to eliminate

trapped air bubbles. The mixture was cured at ambient temperature for 24 hours under controlled pressure to form a single large master slab. From each master slab, nine localized specimens measuring 7x7 cm with a uniform thickness of 3 mm were precisely cut to ensure maximum structural and chemical homogeneity within each experimental batch.

Surface Resistance Measurement

Surface resistance (R*s*) was measured according to ASTM D257 using a digital megohmmeter (Hioki RM3544) at an applied voltage of 500 V DC. Measurements were conducted at ambient room temperature and low relative humidity after 60-second electrification time (ASTM D257-1991, 1991; ASTM D2275-22, 2022). For each of the 18 unique experimental conditions (2 filler sources 9 loading levels), five independent cut specimens were tested to obtain five replicate measurements. These five values were averaged to determine the definitive raw mean surface resistance for that specific concentration profile, serving as the raw dependent variable (Y, measured in Ω) for subsequent statistical modeling (N = 18).

FTIR Spectroscopy

FTIR spectra were acquired using a Thermo Fisher Scientific Nicolet iS20 spectrometer in Attenuated Total Reflectance (ATR) mode, over the wavenumber range 400–4000 cm^{-1} with a resolution of 4 cm^{-1} and 32 scans per spectrum. Peak intensities (absorbance values) at the following characteristic wavenumbers were extracted as independent variables: Si-O-Si (~1010 cm^{-1}), $Si(CH_3)_2$ (~1260 cm^{-1}), $\delta(CH_3)$ (~1410 cm^{-1}), Si-CH_3 (~785 cm^{-1}), ν(Si-C) (~863 cm^{-1}), ν'(Si-C) (~700 cm^{-1}), and C-H (~2960 cm^{-1}) (Nandiyanto et al., 2019; Yang et al., 2021; Zhang et al., 2012). To ensure a tight mathematical pairing between the microscopic chemical descriptors (X) and the macroscopic electrical baseline (Y), a targeted sampling strategy was employed: for each experimental condition, the specific physical specimen whose individual surface resistance value was closest to the batch's calculated mean was selected for FTIR spectral scanning.

Statistical Modeling

The final regression dataset (N = 18) was constructed by pairing the raw mean surface resistance (Y) of the representative specimens with their corresponding vector of filler content percentage (X1) and extracted FTIR absorbance values (X2 to X8). Multiple Linear Regression (MLR) was applied to predict normalized surface resistance values from normalized FTIR absorbance intensities and filler composition. The modelling workflow comprised: (i) Min-Max normalization of all variabel; (ii) Pearson correlation analysis and Variance Inflation Factor (VIF) assessment to detect multicollinearity; (iii) feature selection via Backward Elimination (stepwise removal of non-significant predictors at $\alpha = 0.05$); (iv) introduction of

compound predictors X_9 = [$Si(CH_3)_2$ – Si-O-Si], X_{10} = [2·$Si(CH_3)_2$ – Si-O-Si], and X_{11} = [$Si(CH_3)_2$/Si-O-Si × X_{10}] to capture stoichiometric interactions; and (v) validation via Shapiro-Wilk normality testing of residuals and Bootstrap resampling (n = 2,000 iterations, scikit-learn) for stability assessment (Efron & Tibshirani, 1994; Freund & Wilson, 2003; Wijaya et al., 2024)

Result and Discussion

This section presents a comprehensive evaluation of the chemical, structural, and electrical properties of the fabricated silicone rubber composites, systematically linking experimental characterization with advanced statistical modelling. The discussion begins with the elemental profiling of the two fly ash sources via XRF and the identification of functional groups through FTIR spectroscopy. These chemical benchmarks establish the baseline for analysing variable trends, data normalization, and the subsequent development of Multiple Linear Regression (MLR) models. Furthermore, stoichiometric ratio analysis is employed to evaluate the composition behaviour near the percolation threshold. To ensure the reliability of the predictive models, rigorous validation is conducted through residual analysis and Bootstrap resampling. Finally, the synthesized findings are operationalized into a holistic chemical fingerprint framework designed for quality control applications in composite insulator manufacturing.

XRF Characterization of Fly Ash Sources

The XRF analysis revealed significant compositional differences between the two fly ash sources. The elemental and oxide compositions are presented in Figures 2 and 3, with key oxide percentages summarized in Table 1.

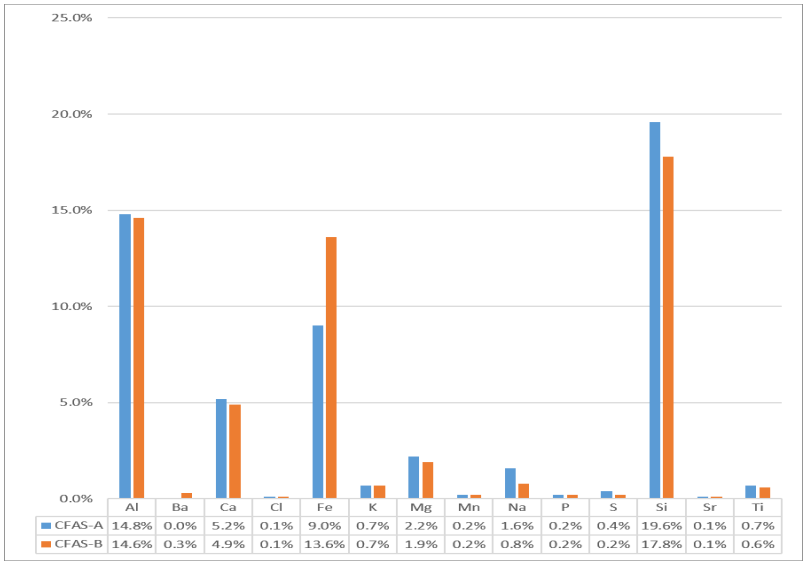

Figure 2 Elemental composition (wt%) of CFAS-A and CFAS-B by XRF analysis

Figure 2 compares the elemental composition (wt%) of CFAS-A and CFAS-B determined by XRF analysis. Both fly ash sources are dominated by silicon (Si) and aluminium (Al). CFAS-A shows modestly higher Si (19.6%) and Al (14.8%) contents, while CFAS-B contains markedly higher iron (Fe) at 13.6% compared to 9.0% in CFAS-A. Other trace elements (Ca, Mg, Na, and Ti) occur in similar minor amounts in both samples.

This elemental profile highlights iron as the most significant point of divergence. The higher Fe content in CFAS-B is particularly noteworthy because iron-rich particles can form localized semi-conductive pathways within the silicone rubber matrix, potentially lowering surface resistance. In contrast, the relatively higher silicon content in CFAS-A is expected to promote better integration with the PDMS polymer network.

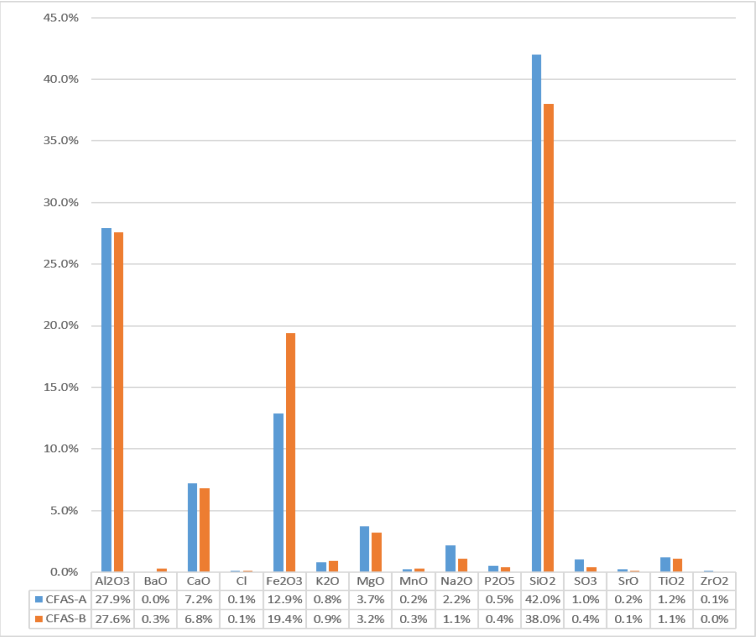

	Al2O3	BaO	CaO	Cl	Fe2O3	K2O	MgO	MnO	Na2O	P2O5	SiO2	SO3	SrO	TiO2	ZrO2
CFAS-A	27.9%	0.0%	7.2%	0.1%	12.9%	0.8%	3.7%	0.2%	2.2%	0.5%	42.0%	1.0%	0.2%	1.2%	0.1%
CFAS-B	27.6%	0.3%	6.8%	0.1%	19.4%	0.9%	3.2%	0.3%	1.1%	0.4%	38.0%	0.4%	0.1%	1.1%	0.0%

Figure 3 Oxide composition (wt%) of CFAS-A and CFAS-B by XRF analysis.

Figure 3 presents the corresponding oxide composition (wt%) of the two fly ash sources. Consistent with the elemental trends, both samples are primarily composed of SiO_2 and Al_2O_3. CFAS-A exhibits higher SiO_2 content (42.0% versus 38.0% in CFAS-B), while CFAS-B contains substantially more Fe_2O_3 (19.4% versus 12.9%). Al_2O_3 concentrations are nearly identical (~27.7%), with only minor differences in other oxides.

These oxide-level differences have important implications for material performance. The elevated SiO_2 in CFAS-A is expected to enhance chemical compatibility with the PDMS matrix and support stable siloxane network formation. Conversely, the higher Fe_2O_3 in CFAS-B may introduce semi-conductive pathways that compromise surface resistance. Such variations help explain the distinct FTIR spectral behaviors and electrical properties between the SRF-A and SRF-B composites.

Table 1 Key Oxide Composition (wt%) of CFAS-A (CFPP) and CFAS-B (Cement)

Oxide	CFAS-A	CFAS-B	Significance
SiO_2	42.0%	38.0%	Higher in CFAS-A → stronger siloxane network
Al_2O_3	27.9%	27.6%	Similar in both sources
Fe_2O_3	12.9%	19.4%	Much higher in CFAS-B → semi-conductive risk
CaO	7.2%	6.8%	Minor difference
MgO	3.7%	3.2%	Minor difference
Na_2O	2.2%	1.1%	Higher alkali in CFAS-A

As shown in Table 1 the substantially higher Fe2O3 content in CFAS-B is a critical concern. Iron oxide exhibits semi-conductive behaviour, with Fe2O3 having an electrical resistivity approximately 10^3–10^5 Ω.cm, which is several orders of magnitude lower than the target insulation resistance. The presence of iron oxide particles can create micro-conductive pathways within the polymer matrix, potentially reducing surface resistance. Conversely, the higher SiO_2 content of CFAS-A (42.0%) is beneficial, as silicon dioxide is chemically compatible with the PDMS matrix, facilitating the formation of siloxane cross-linking bridges that reinforce the polymer network. In contrast, the higher SiO_2 content in CFAS-A (42.0%) is advantageous.

FTIR Spectroscopic Analysis

The evolution of FTIR spectra with increasing fly ash loading for SRF-A and SRF-B composites is illustrated in Figures 4 and 5, respectively. A key difference between SRF-A and SRF-B is observed in the inset regions. In SRF-A (Figure 3, inset at 700–900 cm^{-1}), the Si-CH_3 peak intensity is relatively stable across loading levels, indicating that the methyl groups are well protected by the CFAS-A filler network.

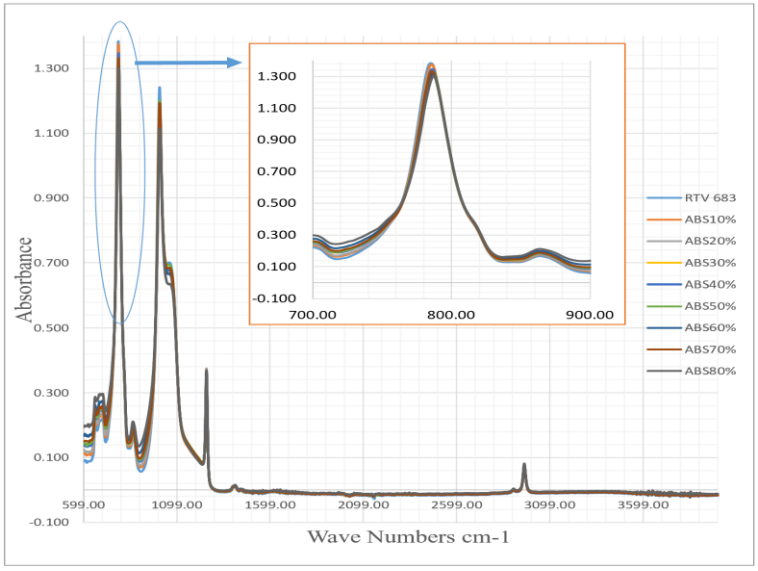

Figure 4 FTIR absorbance spectra of SRF-A composites at filler loadings from 0% (RTV 683) to 80%. Inset shows detail of the 700–900 cm^{-1} region highlighting Si-CH_3 peak evolution

The FTIR spectra of RTV-683 silicone rubber with 0%–80% CSFAS-A fly ash reveal stable chemical backbones, dominated by Si-CH_3 (~785 cm^{-1}) and Si-O-Si (1010–1099 cm^{-1}) peaks. Crucially, increasing filler loading systematically decreases peak intensities (700–900 cm^{-1} region) due to matrix displacement. This quantifiable trend confirms no degradation occurred, validating these absorbance variations for predictive statistical modelling.

In SRF-B (Figure 5, inset at 900–1150 cm^{-1}), the Si-O-Si peak shows more pronounced variation and broadening with loading, consistent with the disruption of siloxane network regularity by the high Fe_2O_3 content in CFAS-B.

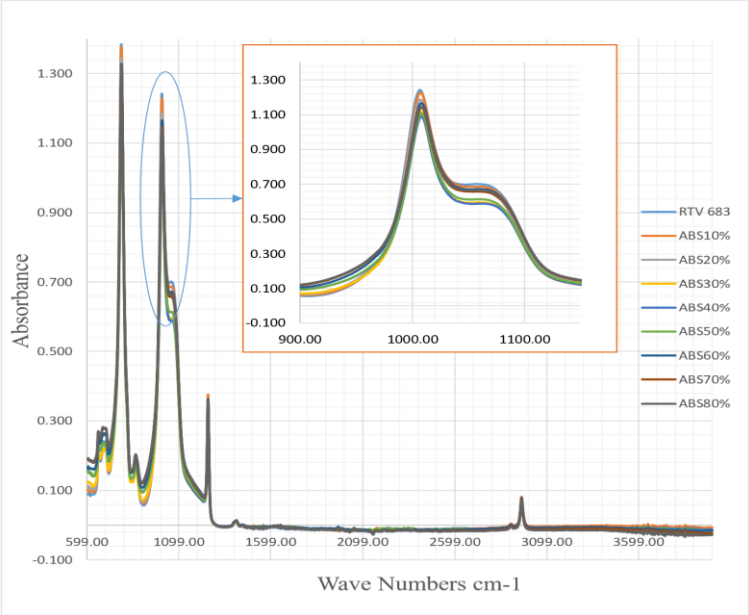

Figure 5 FTIR absorbance spectra of SRF-B composites at filler loadings from 0% to 80%. Inset shows the 900–1150 cm^{-1} region, revealing different Si-O-Si peak behaviour compared to SRF-A.

In both sample groups, the overall spectral profile of PDMS is preserved across all loading levels, confirming that fly ash addition does not permanently alter the fundamental polymer chemistry. However, systematic variations in peak intensities are observed, particularly in the 700–900 cm^{-1} region (inset), reflecting modifications to the local molecular environment.

Table 2 Key FTIR Band Assignments for Silicone Rubber Composites

Wavenumber (cm^{-1})	Assignment	Functional Group	Trend with Loading
~1007–1010	Asymmetric Si-O-Si stretch	Siloxane backbone	Decreasing — Si-O-Si diluted by filler
~1257–1260	$Si(CH_3)_2$ symmetric bend	Dimethyl silyl group	Decreasing in SRF-A; irregular in SRF-B
~785	Si-CH_3 rocking	Methyl-silicon bond	Decreasing; key predictor in SRF-A model
~863	v(Si-C) stretch	Si-C vibration	Increasing — activated by filler interaction

~700	v'(Si-C) stretch	Si-C vibration	Increasing with loading
~1410	δ(CH3) bending	Methyl deformation	Relatively stable
~2962	C-H stretch	Methyl C-H bond	Slightly decreasing

Table 2 details FTIR bands for silicone rubber composites. Increasing fly ash content decreases Si-O-Si (~1010 cm^{-1}), $Si(CH_3)_2$ (~1260 cm^{-1}), and $Si-CH_3$ (~785 cm^{-1}) intensities due to matrix dilution. Conversely, Si-C bands (~863 and ~700 cm^{-1}) increase, indicating filler-polymer interactions. These shifts alter the local molecular environment without destroying the polymer's identity.

Variable Trends and Normalization

The compositional differences observed via XRF are mirrored in the trends of surface resistance and FTIR-derived molecular descriptors across filler loadings for both composite series. In the SRF-A group, surface resistance follows a quadratic-dominant pattern (R^2 = 0.87), peaking near 70–80% loading before a slight decline, consistent with progressive reinforcement of the PDMS network up to a percolation limit as shown in Figure 6.

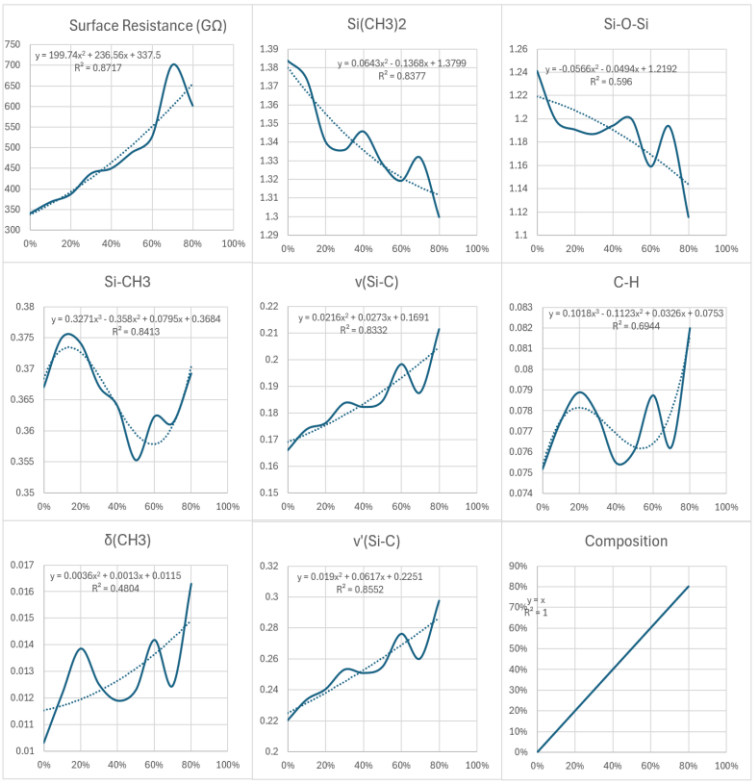

Figure 6 Variable trend analysis for SRF-A: surface resistance (Rs) and FTIR-derived predictors across filler loading levels (0–80%).

The associated FTIR variables (Si(CH3)2, Si-O-Si, Si-CH3, and v(Si-C)) exhibit polynomial trends (R^2 = 0.59–0.87), indicating that electrical performance is closely linked to non-linear changes in polymer chain environment and filler–matrix interactions.

A parallel analysis of the SRF-B series reveals more irregular polynomial behaviour in the same FTIR descriptors (R^2 = 0.57–0.89) as shown in Figure 7. These patterns reflect the disruptive effect of higher Fe_2O_3 content on siloxane network regularity, which helps explain the comparatively modest stoichiometric ratio and slightly lower model performance for SRF-B. Pearson correlation analysis confirmed strong associations (|r| > 0.70) between filler loading and surface resistance in both groups, underscoring concentration as the dominant predictor while highlighting the added value of spectroscopic descriptors in capturing chemistry-specific effects.

Figure 7 Variable trend analysis for SRF-B: surface resistance (Rs) and FTIR-derived predictors across filler loading levels (0–80%).

To prepare for regression modelling, all variables were subjected to min-max normalization. Subsequent multicollinearity diagnostics (VIF) identified strong collinearity between Si-O-Si and Si $(CH_3)_2$ in the combined dataset, leading to the derivation of stoichiometric compound predictors X_9, X_{10}, and X_{11} (Table 3). These adjustments enabled more robust modelling of the interplay between filler chemistry, molecular structure, and macroscopic resistance. Given the modest experimental scale, these trends are interpreted as preliminary evidence rather than definitive thresholds, supporting cautious application in quality control contexts.

Table 3 Compound Predictor Variables Derived from FTIR Stoichiometric Analysis

Variable	Formula	Physical Interpretation
X_9	$[Si(CH_3)_2] - [Si\text{-}O\text{-}Si]$	Simple difference: excess dimethyl silyl over siloxane
X_{10}	$[2 \cdot Si(CH_3)_2] - [Si\text{-}O\text{-}Si]$	Weighted stoichiometric deviation from 2:1 ideal
X_{11}	$[Si(CH_3)_2/Si\text{-}O\text{-}Si] \times X_{10}$	Composite: ratio × stoichiometric deviation

Multiple Linear Regression Models

Feature selection via Backward Elimination yielded distinct optimal model configurations for each data source. The final validated models are summarized in Table 4. The superior performance of model FA1 for SRF-A (Adjusted R^2 = 0.963) compared to SRF-B (FB3, Adjusted R^2 = 0.920) reflects the more regular and predictable chemical structure of CFAS-A composites.

Table 4 Final Regression Model Statistics for SRF-A and SRF-B Composites

Model	Code	Multiple R	R^2	AdjR^2	Std Error	Sig. F	Predictors (p-value)
FA1	SRF-A	0.989	0.97	0.96	22.36	0.000159	Composition (0.00025), $Si\text{-}CH_3$ (0.012), $Si\text{-}O\text{-}Si$ (0.004)
FB3	SRF-B	0.970	0.94	0.92	31.42	0.000215	Composition (0.00023), X_{11} (0.007)
FC2	SRF-AB	0.938	0.87	0.85	42.49	0.000001	Composition (0.00008), ν(Si-C) (0.042), X_{10} (0.020)

The regression equations in original physical units for the two source-specific models are:

SRF-A (Model FA1):

$$R_S = -6816.67 + 788.87 \cdot \text{Composition} + 9213.94 \cdot Si\text{-}CH_3 + 3037.72 \cdot Si\text{-}O\text{-}Si \quad (1)$$

SRF-B (Model FB3):

$$R_S = -3353.31 + 323.91 \cdot \text{Composition} + 2173.88 \cdot X_{11} \quad (2)$$

In model FA1 for SRF-A, the positive coefficients for $Si\text{-}CH_3$ and $Si\text{-}O\text{-}Si$ confirm that higher intensities of these functional group's indicative of a more intact and ordered PDMS network correlate with higher surface resistance. In model FB3 for SRF-B, the dominance of X_{11} as a predictor reflects the importance of the stoichiometric balance between the dimethyl silyl protective groups and the siloxane backbone in determining electrical performance of SRF-B composites. Notably, filler composition (% loading) is the primary predictor in all models ($p < 0.001$), representing the net effect of filler chemistry on polymer structural integrity.

Stoichiometric Ratio Analysis and Percolation Threshold

To further evaluate structural integrity of the PDMS matrix, the covariance ratio of Si (CH3)2 to Si-O-Si relative to surface resistance was calculated across cumulative filler loading ranges as presented in Table 5. This ratio provides a quantitative indicator of how closely the composite approaches the ideal 2:1 dimethyl-to-siloxane stoichiometry of intact PDMS.

Table 5 Surface Resistance-Based Covariance Ratio of Si $(CH_3)_2$: Si-O-Si at Cumulative Loading Ranges

Loading Range	SRF-A Ratio	SRF-B Ratio	Interpretation
0%–20%	0.928	0.964	Both below ideal; initial loading range
0%–30%	1.193	1.010	SRF-A increasing; SRF-B stabilizing
0%–50%	1.644	0.990	SRF-A approaching ideal; SRF-B stagnant
0%–70%	1.921 ★	0.982	SRF-A peak — near-ideal PDMS stoichiometry
0%–80%	1.476 ↓	0.844 ↓	Both decline beyond percolation threshold

★ = peak approaching PDMS ideal ratio 2:1; ↓ = sharp decline beyond 70% percolation threshold

In the SRF-A series, the ratio increased progressively from 0.928 (0–20% loading) to a maximum of 1.921 at 0–70% loading, approaching the theoretical ideal. This trend suggests that the higher SiO_2 content in CFAS-A supports favourable siloxane cross-linking and methyl group stabilization. Conversely, the SRF-B series maintained a lower and relatively stable ratio near 1.0, consistent with greater disruption of polymer chain regularity by the iron-rich CFAS-B filler.

Both composites exhibited a notable decline in the stoichiometric ratio beyond 70% loading (SRF-A: –23%; SRF-B: –14%). This drop, together with reduced statistical significance in the regression models at higher loadings, points to a possible percolation threshold where excessive filler particles begin to interfere with polymer network cohesion. Given the limited sample size, this threshold should be viewed as preliminary rather than definitive. Interestingly, surface resistance in SRF-B continued to rise at 80% loading despite the stoichiometric decline, likely due to physical densification effects rather than improved chemical stability. These findings highlight the complementary roles of filler chemistry and loading level in maintaining molecular-level structural integrity, which in turn influences macroscopic surface resistance.

Residual Analysis and Model Validation

Model assumptions were examined through residual diagnostics and bootstrap validation. Residual scatter plots for the normalized models (A5, B8) and the final models in original units (FA1, FB3) are presented in Figure 8. In all cases, residuals appear randomly distributed around zero with no clear systematic patterns, such as funnel shapes or curvature. This

supports the assumptions of linearity and homoscedasticity across the range of predicted surface resistance values.

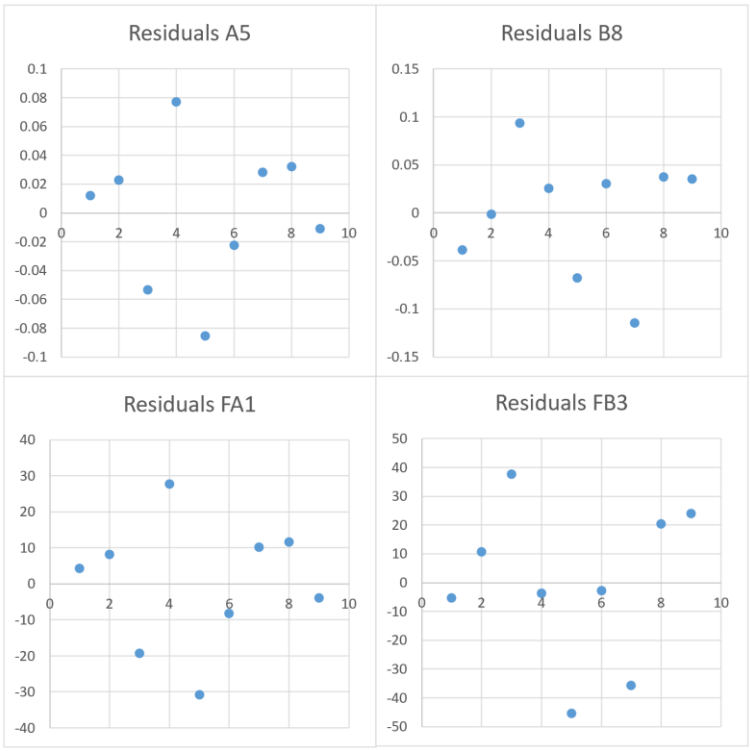

Figure 8 Residual scatter plots for models A5, B8 (normalized data) and FA1, FB3 (original units). Random distribution around zero confirms homoscedasticity.

Normality of residuals was assessed using the Shapiro-Wilk test (Table 6). All models yielded W-statistics (0.944–0.972) well above the critical value (0.829 at $\alpha = 0.05$, $n = 9$), indicating that the residuals follow a normal distribution and supporting the validity of statistical inference from the regression coefficients. To evaluate model stability given the modest sample size (N = 18), a non-parametric bootstrap procedure with 2,000 resampling iterations was performed. The resulting distributions of R^2 values for Models FA1 and FB3 (Figures 9 and 10) demonstrate reasonable robustness. Model FA1 (SRF-A) showed particularly strong stability, with a mean bootstrap R^2 of approximately 0.96 and a tight confidence interval. Model FB3 (SRF-B) exhibited slightly greater variability, consistent with the more heterogeneous nature of the iron-rich filler but still remained within acceptable bounds. These results suggest that the developed models are reasonably stable, though caution is warranted when generalizing beyond the present experimental conditions.

Table 6 Shapiro-Wilk Normality Test Results for Model Residuals

Model	Data Type	W Statistic	Critical W (n=9, α=5%)	Conclusion
A5	Normalized	0.972	0.829	Normal distribution ✓
FA1	Original	0.972	0.829	Normal distribution ✓
B8	Normalized	0.944	0.829	Normal distribution ✓
FB3	Original	0.945	0.829	Normal distribution ✓

Bootstrap Validation

Given the modest sample size (N = 18), bootstrap validation with 2,000 resampling iterations was performed to assess the stability and robustness of the regression models against potential overfitting. The distributions of R^2 values for the final models are shown in Figures 9 and 10, with key metrics summarized in Table 7.

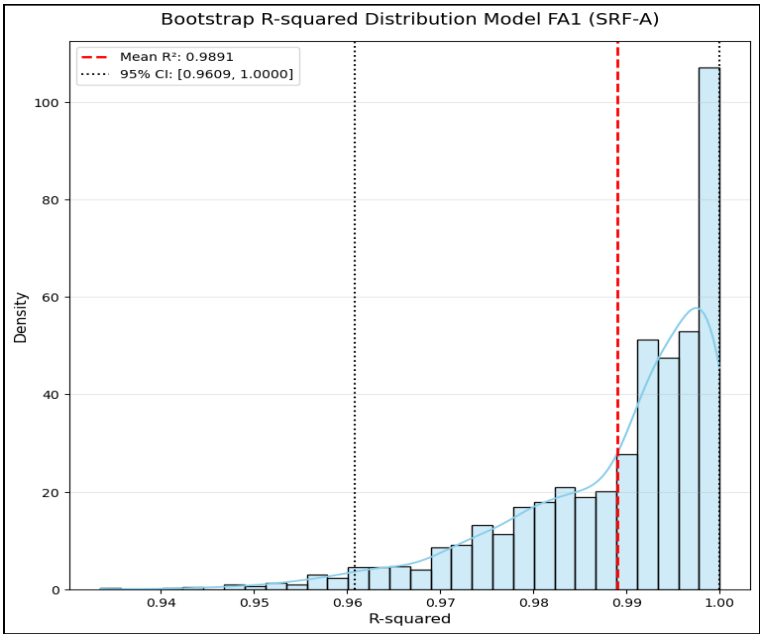

Figure 9 Bootstrap R^2 distribution for predictor-fitted model FA1 (SRF-A)

The bootstrap distribution of R^2 for Model FA1 (SRF-A) is shown in Figure 9. This distribution is strongly skewed toward high values, yielding a high mean bootstrap R^2 and a relatively tight 95% confidence interval. These results indicate good stability for the SRF-A model, in which filler composition together with Si-CH_3 and Si-O-Si intensities reliably predict surface resistance.

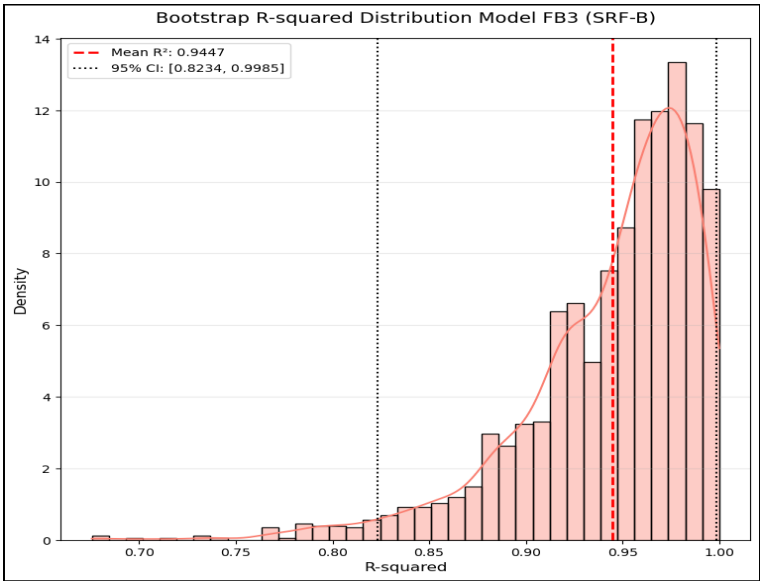

Figure 10 Bootstrap R^2 distribution for predictor-fitted model FB3 (SRF-B)

The bootstrap distribution for Model FB3 (SRF-B) is presented in Figure 10. Compared with the SRF-A model, this distribution exhibits a wider spread and a longer left tail, resulting in a broader confidence interval. While the model remains statistically robust with a mean bootstrap R^2 of 0.8703, the broader distribution suggests that the stoichiometric interactions represented by the X11 predictor are more sensitive to variations in the PDMS matrix than those in the SRF-A series. This variance confirms that the complex interaction between iron-rich phases and polymer surface chemistry introduces a higher degree of stochasticity into the surface resistance behavior.

Table 7 Bootstrap R^2 Summary for Constant-Coefficient Models

Model	Mean R^2 (Bootstrap)	95% CI Lower	95% CI Upper	Stability Assessment
FA1 (SRF-A)	0.9616	0.8392	0.9944	Very high — tight CI, concentrated near 1.0
FB3 (SRF-B)	0.8703	Variable	~0.997	Good — robust, slight long tail in extremes

Key bootstrap metrics for both models are summarized in Table 7. Taken together, the bootstrap metrics for both models confirm that the observed correlations are not artifacts of the small sample size, but rather reflective of genuine physical interactions between filler chemistry and surface resistance. However, the contrast in stability between the two series underscores the importance of filler composition in dictating model predictability. While these findings provide a reliable predictive framework within the current experimental conditions, the increased uncertainty in the SRF-B series highlights a clear boundary for model generalizability. Consequently, the application of these regression models should be approached with caution, particularly when extrapolated beyond the chemical compositions

tested in this study, as the influence of filler heterogeneity may become more significant under broader industrial environments.

Chemical Fingerprint as a Quality Control Framework

The integration of XRF, FTIR spectroscopy, and MLR modeling suggests that the chemical fingerprint of raw fly ash is a critical determinant of long-term composite performance. Data analysis indicates that SiO_2 content of $\geq 42\%$ appears necessary to support the formation of a robust siloxane skeleton. Conversely, iron-rich fillers—such as the CFAS-B cohort—demonstrate that Fe_2O_3 concentrations exceeding 15% may facilitate the formation of micro-conductive pathways, which likely disrupt the local electric field and accelerate tracking degradation. These findings suggest that filler mineralogy directly dictates the susceptibility of the insulation surface to high-voltage stress. Furthermore, the Stoichiometric Stability Index reveals a strong correlation between the polymer matrix integrity and the ratio of $Si(CH_3)_2$ to Si-O-Si units. Experimental results show that a deviation from the baseline ratio (approaching 1.0 in the CFAS-B composite) corresponds with a compromised polymer shield, likely due to filler interference with the cross-linking process. This suggests that the hydrophobic integrity of the surface is intimately tied to the retention of $Si-CH_3$ functional groups, which are susceptible to dilution as filler loading increases.

Finally, the modeling results highlight a structural percolation threshold at 70 wt%. At this concentration, the sharp decline in the stoichiometric ratio suggests a structural collapse where the PDMS matrix can no longer effectively encapsulate filler particles, leading to agglomeration and potential internal voids. While these correlations provide a compelling basis for understanding the structure-property relationships within the measured samples, the limited experimental dataset necessitates caution. The proposed thresholds should be regarded as preliminary indicators of material limits rather than definitive industrial standards, requiring further verification across broader chemical compositions.

Conclusions

This study established a chemical fingerprinting approach—integrating FTIR spectroscopy and Multiple Linear Regression (MLR)—to evaluate the structure-property relationships of coal fly ash-filled silicone rubber insulators. The analysis confirms that filler chemistry, particularly the balance between SiO_2 and Fe_2O_3 content, is a primary determinant of surface resistance behavior. Specifically, the retention of the ideal stoichiometric ratio of dimethyl silyl groups to siloxane bridges serves as a sensitive indicator of polymer network integrity, which significantly degrades when iron-rich filler concentrations compromise the matrix. Furthermore, the identification of a 70 wt% percolation threshold provides a physical

boundary for maintaining structural cohesion in these composites. While these findings highlight the potential for using chemical fingerprints as a non-destructive quality assessment tool, the proposed framework is derived from a limited experimental dataset. Consequently, these metrics should be interpreted as preliminary indicators of material limits rather than definitive industrial standards. Future research is required to validate these correlations across a wider array of filler compositions and to assess their stability under long-term environmental aging, which remains essential for transitioning these laboratory findings into robust industrial applications.

References

Apriyanti, E., Chasanah, U., & Subekti, S. (2024). Pemanfaatan material komposit fly ash sebagai bahan substitusi pada pembuatan beton ditinjau dari uji tekan dan uji porositas. Jutsu : Jurnal Teknik Sipil Unpand, 1(2), 146–153. https://doi.org/10.69796/axb1yh47

Asof, M., Arita, S., Luthfia, L., Andalia, W., & Naswir, M. (2022). Analisis karakteristik dan potensi logam pada limbah padat fly ash dan bottom ash di PLTU industri pupuk. Jurnal Teknik Kimia, 28(1), 44–50. https://doi.org/10.36706/jtk.v28i2.977

ASTM D257-1991. (1991). ASTM D257: Standard Test Method for DC Resistance of Conductance of Insulating Materials: American Society for Testing and Materials : Free Download, Borrow, and Streaming : Internet Archive. https:// archive.org/deta ils/gov.law.astm.d257.1991

ASTM D2275-22. (2022). Test Method for Voltage Endurance of Solid Electrical Insulating Materials Subjected to Partial Discharges (Corona) on the Surface. ASTM International. https://doi.org /10.1520/D2275-22

Chinara Abinawa, & Alieftiyani Paramita Gobel. (2024). Studi Pengolahan Limbah Fly Ash Batubara dalam Upaya Peningkatan Konsentrasi Silika Menggunakan Asam Sitrat. INSOLOGI: Jurnal Sains Dan Teknologi, 3(3), 288–296. https://doi .org/10.55 123/insologi.v3i3.3519

Christiono, C. (2017). Kinerja Isolasi Polimer Silicone Rubber Berbahan Pengisi Fly Ash Batu Bara Di Bawah Pengaruh Iklim Tropis. https://repository.unhas.ac.id/id/eprint/28239/1/CHRISTIONO_P2700214046_KINERJA%20ISOLASI%20POLIMER%20.pdf

Christiono, R., Iwa Garniwa M, K., Fikri, M., Thahara, A. A., & Putra, R. P. (2023). Optimization of Coal Fly Ash Filler Effect on Polymer Silicone Rubber Base Insulator Material on Dielectric Performance. 2023 4th International Conference on High Voltage Engineering and Power Systems (ICHVEPS), 705–710. https://doi.org/10.1109/ICHVEPS58902.2023.10257370

DJMB. (2021). Road Map Pengembangan dan Pemanfaatan Batubara 2021-2045. Kementerian Energi dan Sumber Daya Mineral Direktorat Jenderal Mineral dan Batubara. https://www.esdm.go.id/assets/media/content/content-buku-road-map-pengembangan-dan-pemanfaatan-batubara.pdf

Efron, B., & Tibshirani, R. J. (1994). An Introduction to the Bootstrap. Chapman and Hall/CRC. https://doi.org/10.1201/9780429246593

Fan, S., Zhang, X., Lu, Y., & Gao, Y. (2018). Characterization of HTV silicone rubber with different content of ATH filler by mechanical measurements, FTIR and XPS analyzes. 2018 12th International Conference on the Properties and Applications of Dielectric Materials (ICPADM), 888–891. https://doi.org/10.1109/ICPADM.2018.8401171

Ferdyanto, M., & Afriandini, B. (2023). Pemanfaatan Limbah Asbes dan Fly Ash Sebagai Bahan Tambah Campuran Beton. Reviews in Civil Engineering, 7(1), 1–6. https://doi.org/10.31002/rice.v7i1.385

Fikri, M., Christiono, M.K, I. G., Abduh, S., Sari, K. J., Raafid, H., An'nafri, D. S., & Romadhoni, M. L. (2024). The Effect of Addition of Coal Fly Ash as Filler in Silicone Rubber Polymer Isolator Materials on the Characteristics of Tensile Strength and Elongation. 2024 International Conference on Technology and Policy in Energy and Electric Power (ICTPEP), 166–169. https://doi.org/10.1109/ICT-PEP 6382 7.202 4.1 0733400

Freund, R. J. ., & Wilson, W. J. . (2003). Statistical methods. Academic Press.

K. K. Kar.(2022). *Handbook of Fly ash*. Butterworth-Heinemann, an imprint of Elsevier,

Ikhlas Kitta, Salama Manjang, Wihardi Tjaronge, & Rita Irmawaty. (2016). Performance Study of Silicone Rubber Polymer was Filled Fly Ash as Insulator Material on High Voltage Transmission Tower. International Journal of Innovative Research in Advanced Engineering, 3(1). https://www.ijirae.com/volumes/Vol3/iss1/09.JAAE10093.pdf

Kitta, I., Manjang, S., Tjaronge, W., & Irmawaty, R. (2016a). Effect of Coal Fly Ash Filler in Silicone Rubber and Epoxy Resin as Insulating Material in Wet Environmental Conditions. 16(2). https://scholar.unhas.ac.id/en/publications/effect-of-coal-fly-ash-filler-in-silicone-rubber-and-epoxy-resin-/

Kitta, I., Manjang, S., Tjaronge, W., & Irmawaty, R. (2016b). Effect Of Fly Ash Filler To Dielectric Properties Of The Insulator Material Of Silicone Rubber And Epoxy Resin. 5(3).

Nandiyanto, A. B. D., Oktiani, R., & Ragadhita, R. (2019). How to Read and Interpret FTIR Spectroscope of Organic Material. Indonesian Journal of Science and Technology, 4(1), 97. https://doi.org/10.17509/ijost.v4i1.15806

Nurfitria, N., & Febriyantiningrum, K. (2023). Studi Potensi Pemanfaatan Limbah Fly Ash Batu Bara Berdasarkan Kajian Parameter Kimia. Biology Natural Resources Journal, 2(2), 75–79. https://doi.org/10.55719/binar.v2i2.723

Purnamasari, E., Antonius, & Setiyawan, P. (2025). Analisis Penggunaan Fly Ash Tipe F pada Beton Non Pasir sebagai Green Concrete. Science Tech: Jurnal Ilmu Pengetahuan Dan Teknologi, 11(1). https://doi.org/10.30738/st.vol11.no1.a19194

Rafrita, F. K., Anwar, S. N. R., & Umniati, B. S. (2023). Sifat Mekanik Bata Ringan Geopolimer Berdasarkan Rasio Si/AL. Bentang : Jurnal Teoritis Dan Terapan Bidang Rekayasa Sipil, 11(2), 179–188. https://doi.org/10.33558/bentang.v11i2.6773

Roesdiono, C., Garniwa, I. M. K., & Setiabudy, R. (2025). Review of Dielectric Properties Optimization of RTV Silicone Rubber Using Coal Fly Ash Filler with the Backpropagation Neural Network-Genetic Algorithm Method. Multiscale and Multidisciplinary Modeling, Experiments and Design 2025 9:1, 9(1), 62-. https://doi.org/10.1007/s41939-025-01134-1

Syahputra, M. B., Jati, D. R., & Saziati, O. (2023). Identifikasi Potensi Abu Terbang (Fly Ash) Sebagai Bahan Pengganti Sebagian Semen Pada Pembuatan Paving Block Ramah Lingkungan. Jurnal Teknologi Lingkungan Lahan Basah, 11(3), 620–627. https://doi.org/10.26418/jtllb.v11i3.67931

Syamsir Abduh. (2003). Teori Kegagalan Isolasi. Penerbit Universitas Trisakti.

Tambunan, P. M. (2022). Karakterisasi Kadar Mineral, Logam Berat Serta Distribusi Ukuran Partikel Limbah Abu Terbang (Fly Ash) Sisa Pembakaran Batu Bara Industri Oleokimia. Journal of The Indonesian Society of Integrated Chemistry, 14(2), 100–108. https://doi.org/10.22437/jisic.v14i2.21355

Thahara, A. A., Fatah, M. C., Mulyana, I. G., Tio, C., & Fikri, M. (2023). Optimasi Dielektrika Isolator Polimer Silicone Rubber menggunakan Bahan Pengisi Limbah Coal Fly Ash. ELKOMIKA: Jurnal Teknik Energi Elektrik, Teknik Telekomunikasi, & Teknik Elektronika, 11(4), 1075. https://doi.org/10.26760/elkomika.v11i4.1075

Wijaya, E., Degdo Suprayitno Urwawuska Ladini, M., Titin Agustin Nengsih, Ms., Sella Nofriska Sudrimo, M., Sri Yani Kusumastuti Nurhayati, Ms., & Dalizanolo Hulu, M. (2024). BUKU AJAR EKONOMETRIKA. www.buku.sonpedia.com

Yang, H., Wen, R., Zhao, H., Guo, M., Zhang, L., & Chen, Y. (2021). Study on ageing characteristics and evaluation methods of RTV silicone rubber in high humidity area. PLOS ONE, 16(6), e0251092. https://doi.org/10.1371/journal.pone.0251092

Zhang, H., Tu, Y., Lu, Y., Xu, Z., Chen, C., & Xie, L. (2012). Study on aging characteristics of silicone rubber insulator sheds using FTIR. 2012 IEEE International Symposium on Electrical Insulation, 83–86. https://doi.org/10.1109/ELINSL.2012.6251431